Desalination and Water Treatment
www.deswater.com
doi: 10.1080/19443994.2013.871343

53 (2015) 2980–2989
March

Taylor & Francis
Taylor & Francis Group

Enhancement of adsorption efficiency of methylene blue on Co_3O_4/SiO_2 nanocomposite

Hany H. Abdel Ghafar[a,b,*], Gomaa A.M. Ali[c,d], Osama A. Fouad[e], Salah A. Makhlouf[f,g]

[a]*Faculty of Science and Arts, Department of Chemistry, King Abdulaziz University, Khulais, Saudi Arabia*
Tel. +996 533645049; email: hany_ghafar@hotmail.com
[b]*Water Pollution Research Department, National Research Center, Cairo 12311, Egypt*
[c]*Faculty of Science, Chemistry Department, Al-Azhar University, Assiut branch, Assiut 71524, Egypt*
[d]*Faculty of Industrial Science and Technology, University Malaysia Pahang (UMP), Kuantan 26300, Pahang, Malaysia*
[e]*Central Metallurgical Research and Development Institute, CMRDI, P.O. Box 87, Helwan 11421, Egypt*
[f]*Faculty of Science, Physics Department, Assiut University, Assiut 71516, Egypt*
[g]*Deanship of Scientific Research, Al Imam Mohammad Ibn Saud Islamic University (IMSIU), Riyadh 11463, Saudi Arabia*

Received 24 July 2013; Accepted 21 November 2013

ABSTRACT

Single and well-crystalline Co_3O_4 phase imbedded in an amorphous SiO_2 matrix has been obtained by novel aqueous solution method. The structural and morphological properties are investigated using X-ray diffraction, Fourier transform infrared spectrometer, and N_2 adsorption–desorption techniques. The apparent crystallite size for Co_3O_4 was found to be about 13.5 nm, which elucidates the rule of poly ethylene glycol in preventing particle's agglomeration; moreover, the pours structure of the composite enhances its adsorption ability. Co_3O_4/SiO_2 has a high ability to absorb methylene blue from an aqueous solution. The removal percent of Methelene blue (MB) by Co_3O_4/SiO_2 has reached 95.7%. The effect of various experimental parameters, such as initial dye concentration, contact time, and dose were investigated. Co_3O_4/SiO_2 nanocomposite shows high adsorption capacity of 53.87 mg g^{-1}, which is larger than the adsorption capacity of MB on other materials. Both of Langmuir and Freundlich models were used to analyze the equilibrium adsorption data. The pseudo-second-order model was found to be the most appropriate model to represent the present data. Co_3O_4/SiO_2 nanocomposite material is proposed as a potential adsorbent for water treatment.

Keywords: Cobalt Oxide/Silica; Nanocomposite; Adsorption; Methylene blue

1. Introduction

One of the important applications of metal oxide/silica nanocomposites is employing them in the field of catalysis. For instance, silica-supported cobalt has been reported as an excellent catalyst [1–3]. Moreover, these nanocomposites have excellent surface properties making them potential humidity sensor materials [4]. Silica is commonly used as a supporting material because of its ability to prevent the core nanoparticles from leaching in an acid environment [5], inhibit the growth of the core nanoparticles, and stabilize their crystalline structure [6], increase their thermal stability [7,8], and enhance the void fraction [4,9].

*Corresponding author.

Large surface/volume ratio with decreasing particle size in nanocomposites makes them highly reactive catalysts. Co/SiO_2 catalyst does not require long activation treatments prior to use and it is stable under process cycles [10]. Co/SiO_2 is used as a catalyst in many reactions and chemical process such as heterogeneous autoxidation of α-pinene into valuable oxygenated derivatives [1], Fischer–Tropsch synthesis [11], and aerobic epoxidation of olefins [12]. Besides the wide range of applications of dyes and pigments in many fields such as the textiles, paper, plastics, leather, food, and cosmetic industry, they may on the other hand reduce light penetration and photosynthesis when they present in wastewater. Moreover, dyes are considered as one of the sources of pollution and eutrophication.

Biodegradation [13], flocculation–coagulation [14], chemical oxidation [15], and adsorption [16] are the main techniques that can be used for treatment of wastewater containing dyes. Adsorption has been found to be the most effective and economic alternative with high potential for the removal and recovery of dyes from wastewater [17,18]. Methylene blue (MB) has wide applications, which include coloring paper, dyeing cottons, wools, and coating for paper stock [18].

In this paper, Co_3O_4/SiO_2 nanocomposite has been prepared by novel aqueous solution method. The sample was characterized by X-ray diffraction (XRD), Fourier transform infrared spectrometer (FTIR), and N_2 adsorption–desorption techniques. Removing of MB from an aqueous solution by Co_3O_4/SiO_2 nanocomposite was investigated. The kinetics and adsorption equilibrium of the basic dye were discussed. The results show that Co_3O_4/SiO_2 nanocomposite is an effective adsorbent for removing the dye.

2. Experimental procedures and techniques

2.1. Sample preparation

2.1.1. Materials

Cobalt(II) chloride ($CoCl_2{\cdot}6H_2O$) was used as a source of Co, sodium silicate ($Na_2SiO_3{\cdot}9H_2O$) was used as a source of SiO_2, poly ethylene glycol (PEG, $C_2H_5O(C_2H_4O)_nOC_2H_5$) was used as a capping agent, sodium hydroxide (NaOH) was used as a pH adjustor, and doubly distilled water (H_2O) was used as solvent.

MB has a molecular weight of 319.9 g mol^{-1}, which corresponds to MB hydrochloride. The structure of MB is as follows:

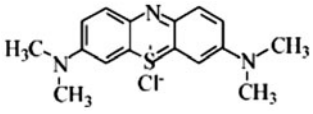

2.1.2. Procedure

To obtain powder Co_3O_4/SiO_2 nanocomposite, NaOH solution (10%) was added to an aqueous solution of $CoCl_2{\cdot}6H_2O$ with continuous stirring. The stirring speed was fixed at about 1,500 rpm. The mixture was kept for 30 min at room temperature with pH of about 12. PEG (2 ml, 10%) was added dropwise to this solution for preventing particle's agglomeration. An aqueous solution with a calculated amount of $Na_2SiO_3{\cdot}9H_2O$ was added such as to control the ratio of $Co{:}SiO_2$ at the desired weight ratio (25 wt.%). The mixture was dissolved ultrasonically. The suspension was repeatedly washed, filtered for several times, and dried at 80°C in a drying oven for 24 h. The dried powder was then calcined at 400°C for 3 h. The main synthesis steps are further illustrated in Fig. 1.

2.2. Sample characterizations

The obtained phase was examined by powder XRD (Philips PW1700 diffractometer, Netherlands).

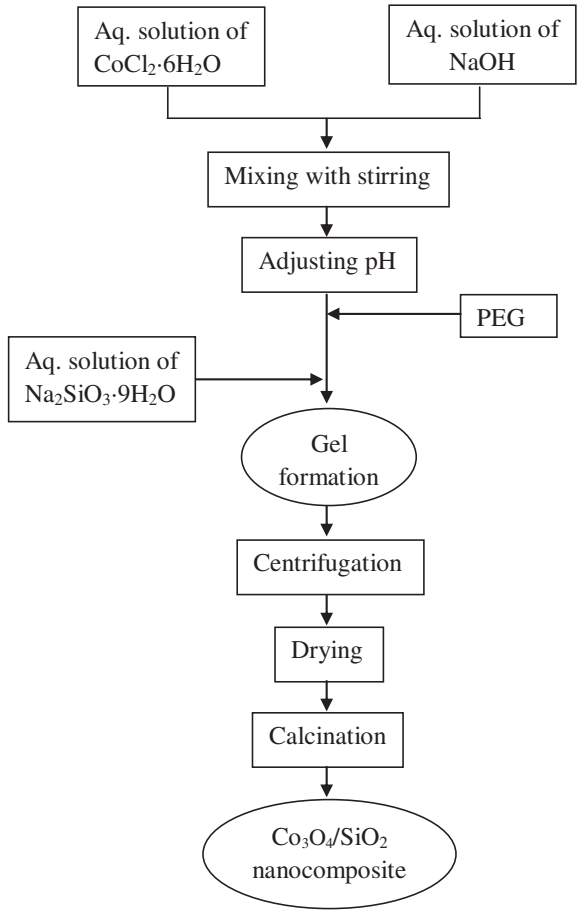

Fig. 1. Preparation scheme for Co_3O_4/SiO_2 nanocomposite.

Diffraction patterns were obtained using Cu-Kα radiation ($\lambda = 0.15418$ nm) and a graphite monochromator in the 2θ range from 10° to 80°. XRD patterns are fitted and analyzed using pseudo-Lorentzian line shape, as described elsewhere [4,8]. Infrared spectra were measured in the range 4,000–400 cm^{-1} using a FTIR (JASCO-480 Plus, Japan).

The specific surface area, pore volume, and pore size distribution of the sample were measured by nitrogen adsorption–desorption technique (NOVA-3200, USA).

2.3. Batch adsorption experiments

Each batch for adsorption study was carried out by contacting the Co_3O_4/SiO_2 nanocomposite material with MB in 100 ml stopper conical flask. The experiments were conducted at room temperature (25 ± 0.1°C) and normal pH to determine the effects of adsorbent dosage, contact time, and initial concentration on the adsorption of MB. Each experiment was conducted in a mechanical shaker at 120 rpm. The samples were filtered through Whatman filter paper (No. 41) and the MB concentration was determined in the filtrate. The residual MB concentrations were measured using a UV-vis spectrophotometer (Jasco, V-530, Japan) at 665 nm (λ_{max} of MB). All experiments were carried out in triplicate and the mean of the quantitative results were used for further calculations. To calculate the mean value, the percent relative standard deviation for the results was obtained, and the data were discarded if its value for a given sample was greater than 5%.

2.3.1. Effect of contact time

The optimum time was carried out by conducting batch adsorption experiments with an initial MB concentration of 20 mg L^{-1}, 0.8 g L^{-1} adsorbent dosage, and at different time periods of 5, 10, 15, 20, 30, 40, and 60 min.

2.3.2. Effect of adsorbent dosage

The adsorbent dosage varied from 5 to 50 mg using a fixed volume of 50 mL of 20 mg L^{-1} of MB solution at the equilibration time.

2.3.3. Adsorption isotherms

Isotherms were measured by varying the initial MB concentrations at the optimum conditions. Different adsorption models were used for comparison with the experimental data.

3. Results and discussion

Cobalt chloride was converted into cobalt hydroxide using sodium hydroxide. Silica hydrogels were prepared by hydrolysis of sodium silicate sol. The hydrolysis and condensation reactions occurred during hydrogel formation are as follows [19]:

Hydolysis:

$$CoCl_2 + 2NaOH \rightarrow Co(OH)_2 + 2NaCl \quad (1)$$

$$Na_2SiO_3 + 3H_2O \rightarrow Si(OH)_4 + 2NaOH \quad (2)$$

Calcination:

$$3Co(OH)_2 + \frac{1}{2}O_2 \xrightarrow{400\,^{\circ}C} Co_3O_4 + 3H_2O \quad (3)$$

$$Si(OH)_4 \xrightarrow{400\,^{\circ}C} SiO_2 + 2H_2O \quad (4)$$

3.1. X-ray diffraction

Fig. 2 shows the XRD pattern of the nanocomposite after thermal annealing at 400°C for 3 h. The diffraction peaks reveal the formation of a spinel type fcc crystalline lattice of Co_3O_4 nanoparticles (JCPDS card # 78-1970). In addition, the peaks are broad implying the nanoscale particle size. The weak and broad peak at $2\theta \approx 16^{\circ}$ in the XRD pattern was ascribed to SiO_2 phase (JCPDS card # 86-0681). No other diffraction peaks corresponding to silica matrix were observed indicating that silica presents in the amorphous form. The apparent crystallite size was calculated using Debye–Scherrer formula (Eq. (5)).

$$PS_{XRD} = \frac{k\,\lambda}{\beta\,\cos\theta} \quad (5)$$

where k is constant equals 0.9, λ is wavelength of the radiation, β is the full width at half maximum intensity in radians, and θ is the Bragg angle.

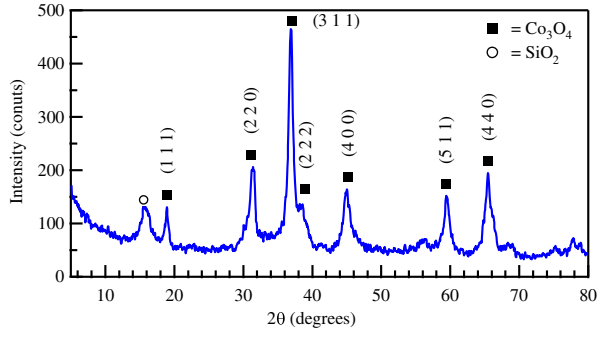

Fig. 2. XRD pattern of Co_3O_4/SiO_2 nanocomposite.

The apparent crystallite size for Co_3O_4 was found to be about 13.5 nm, which elucidates the rule of PEG in preventing the particles from agglomeration. Similar results were previously obtained when using ethylene glycol and citric acid as capping agents [4]. The lattice constant (a) and the cell volume (V) were calculated using a least squares refinement program [20], showing that Co_3O_4 has $a = 8.071$ Å and $V = 525.75$ Å^3.

3.2. FTIR spectra

Fig. 3 shows the FTIR spectrum of Co_3O_4/SiO_2 nanocomposite, calcined at 400°C for 3 h. It is obvious that the absorption bands at 3,440 and 1,635 cm^{-1} belong to stretching and bending vibrational modes of O–H of molecular water. These two bands may be attributed, respectively, to stretching and bending vibrational modes of O–H of the Si–OH stretching of surface silanol hydrogen bond to molecular water [21,22]. The strong IR absorption bands at 1,090 and 800 cm^{-1} agree well with the SiO_2 bond structure. The band at 1,090 cm^{-1} can be assigned to the asymmetric stretching vibration of the bond Si–O–Si in the SiO_4 tetrahedron. The band at 800 cm^{-1} is corresponding to the vibration of the Si–O–Si symmetric stretch. The band at 460 cm^{-1} is associated with the stretching vibration of Si–O–Si mode. The absorption band at 660 cm^{-1} is related to the vibrations of Co^{III}–O bonds in Co_3O_4. This band was alternatively assigned to be associated with the Co–O stretching in Si–O–Co network by other authors [7,8]. The band at 560 cm^{-1} that also associated with the Co–O stretching is also confirmed.

3.3. N_2 adsorption–desorption technique

Fig. 4 shows the N_2 adsorption–desorption isotherm for Co_3O_4/SiO_2 nanocomposite, calcined at 400°C for 3 h. The isotherms can be classified; according to the IUPAC [23], as type IV that characterizes a mesoporos material which has a high energy of adsorption. The specific surface area (S_{BET}, 23.7 m^2 g^{-1}) was obtained from the N_2 adsorption–desorption data. The equivalent spherical particle size (PS_{BET}) of the composite expressed in nanometers was estimated assuming spherical shape of the particles and by using Eq. (6) as [4]:

$$PS_{BET} = \frac{6000}{S_{BET}\ \rho_B} \tag{6}$$

where ρ_B is the density of bulk composite in g cm^{-3} calculated using the weight ratio of each phase in the sample. The obtained PS_{BET} value was found to be 83.8 nm.

Average pore width (P_w) was estimated using Eq. (7) as [4]:

$$P_w = \frac{4\,V_p}{S_{BET}} \tag{7}$$

where V_p is the pore volume. The P_w value was 5.4 nm. Porosity is a measure of the void spaces in the material, and it is a fraction of the volume of voids over the total volume. The void fraction (or porosity) of the silica particles (ε) was calculated using Eq. (8) as [4,9]:

$$\varepsilon = \frac{V_p}{V_p + 1/\rho_{app}} \tag{8}$$

where V_p is the pore volume ($cm^3\,g^{-1}$) and ρ_{app} is the apparent density (g cm^{-3}) of silica particles. For the present silica matrix, ε was found to be 0.08.

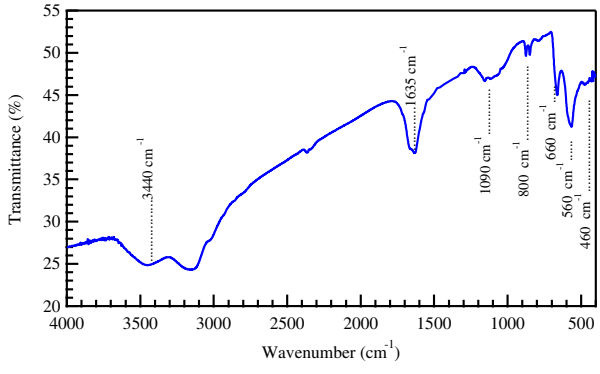

Fig. 3. FTIR spectrum of Co_3O_4/SiO_2 nanocomposite.

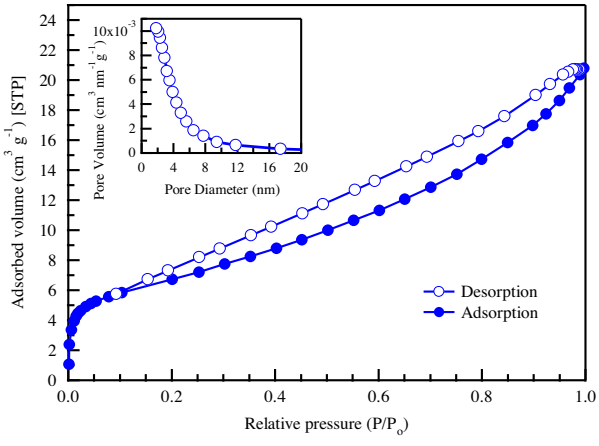

Fig. 4. N_2 adsorption–desorption isotherm of Co_3O_4/SiO_2 nanocomposite.

3.4. MB removal by Co_3O_4/SiO_2 nanocomposite

The removal percent (R) was calculated using Eq. (9) as [24]:

$$R = \frac{C_i - C_f}{C_i} \times 100 \quad (9)$$

where C_i and C_f are the concentrations of MB in initial and final solutions, respectively. The amount of MB adsorbed Q (mg g^{-1}) was calculated from the mass balance equation as given by Eq. (10) [16]:

$$Q = \frac{C_i - C_f}{W} \quad (10)$$

where W is the mass of Co_3O_4/SiO_2 sample used in grams.

3.4.1. Effect of adsorbent dosage

The adsorbent dosage in solution plays an important role in the dye uptake as well as in the percentage of color removal. The effect of different dosages on MB removal was carried out. The results are shown in Fig. 5(A) for the following parameters: time 60 min, MB concentration 20 mg L^{-1}, 50 mL solution, constant temperature, and normal pH. It is obvious that the MB removal percentage increases with increasing Co_3O_4/SiO_2 dose. Increasing the adsorbent dose serves to increase the surface area and the number of active sites for adsorption. The removal percent of MB for 20 mg L^{-1} reached 95.7% using 40 mg of Co_3O_4/SiO_2 (0.8 g L^{-1} as optimum dose). Therefore, a 40 mg (0.8 g L^{-1}) sample was used in the rest of experiments as an optimum dose.

3.4.2. Effect of contact time

The effect of contact time on adsorption of MB onto Co_3O_4/SiO_2 was studied at a dose of 40 mg, MB concentration 20 mg L^{-1}, 50 mL volume, constant temperature, and normal pH. The results are shown in Fig. 5(B) (left vs. bottom). It is apparent that the adsorption gradually increases with increasing the contact time. The time requires to reach equilibrium is 30 min. The initial rapid increase in the removal rate is due to the effect of functional groups on the surface of adsorbent. The porous nature of Co_3O_4/SiO_2 nanocomposite play an important role in the adsorption process, where the adsorption of MB was thought to take place probably via surface adsorption until the surface functional sites were fully occupied, thereafter; MB molecules diffuse into the pores of the adsorbents facilitating further adsorption. Similar features were observed for these nanocomposites in case of water vapor adsorption [4].

3.4.3. Effect of MB concentration

The data presented in Fig. 5(B) (left vs. top) shows the effect of MB concentration on the adsorption process. The concentration of MB was varied from 5 to 30 mg L^{-1} at the optimum parameters (40 mg adsorbent dose and 30 min contact time), constant temperature, and normal pH. The results are presented in Fig. 5(B) (left vs. top), and indicate that the adsorption of MB at the beginning was 96.5%. The adsorption increases with increasing the MB concentration from 2 to 10 mg L^{-1}, and becomes constant with increasing MB concentration further. This behavior was attributed to the fact that, initially, all binding sites on the adsorbent surface were vacant leading to MB adsorption on the surface of adsorbent. With further increase of MB concentration, the adsorption of MB slightly increases in account to the few active sites available on the surface, and after that MB molecules diffuse into the pores of the adsorbent for further adsorption.

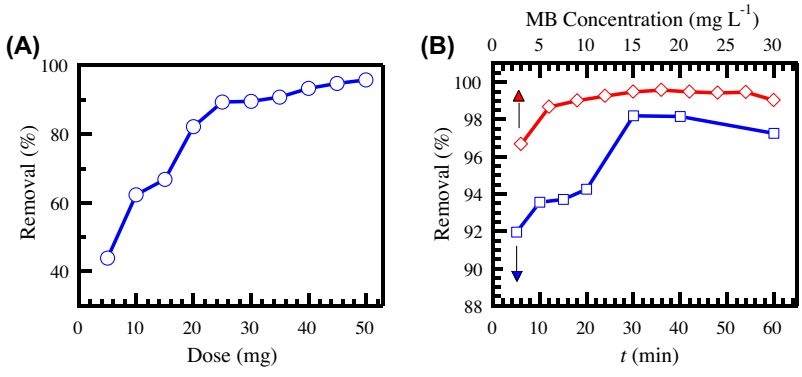

Fig. 5. Effect of (A) dose and (B) time (left vs. bottom) and concentration (left vs. top) on the removal of MB.

3.4.4. Adsorption isotherms

Several mathematical models have been used to describe equilibrium states for the adsorption of dyes on solid surfaces. Freundlich and Langmuir models are frequently utilized to describe the experimental data.

3.4.4.1. Freundlich isotherm. Freundlich isotherm gives the relationship between equilibrium liquid and solid phase capacity based on the multilayer adsorption (heterogeneous surface). This isotherm is derived assuming that the adsorption sites are distributed exponentially with respect to the heat of adsorption and is given by Eq. (11) as [17,25]:

$$\log Q = \log K_F + \frac{1}{n}\log C_e \tag{11}$$

where C_e is the equilibrium concentration of the MB in the solution (mg L^{-1}), K_F and n are Freundlich constants. The dimensionless constant n is an indication of how favorable the adsorption process, whereas K_F is the adsorption capacity of the adsorbent. Fig. 6(A) shows a plot of log Q vs. log C_e, where a straight line is obtained. The values of n and K_F were found to be 0.813 and 587.89 mg g^{-1} (L $mg^{-1})^{1/n}$, respectively, as displayed in Table 1.

3.4.4.2. Langmuir isotherm. The Langmuir model, on the other hand, assumes that the adsorption occurs on a homogenous surface and no interaction between adsorbates in the plane of the surface. Langmuir isotherm is formulated by Eq. (12) as [17,25]:

$$\frac{C_e}{Q} = \frac{1}{Q_{\max} K_L} + \frac{C_e}{Q_{\max}} \tag{12}$$

where $Q_{\max}$ is the maximum adsorption capacity (mg g^{-1}) and K_L is a Langmuir constant related to the affinity of the binding sites and energy of adsorption (L mg^{-1}). Linear relation of Ce/Q vs. C_e was obtained, as shown in Fig. 6(B). $Q_{\max}$ of 53.87 mg g^{-1} or 1.665×10^{-4} mol g^{-1} and K_L of 8.39 L mg^{-1} were obtained from the intercept and slope, respectively. The MB maximum adsorption capacity of Co_3O_4/SiO_2 nanocomposite is 53.87 mg g^{-1}, which is larger than the adsorption capacity of MB on coir pith carbon (5.87 mg g^{-1}) [17],

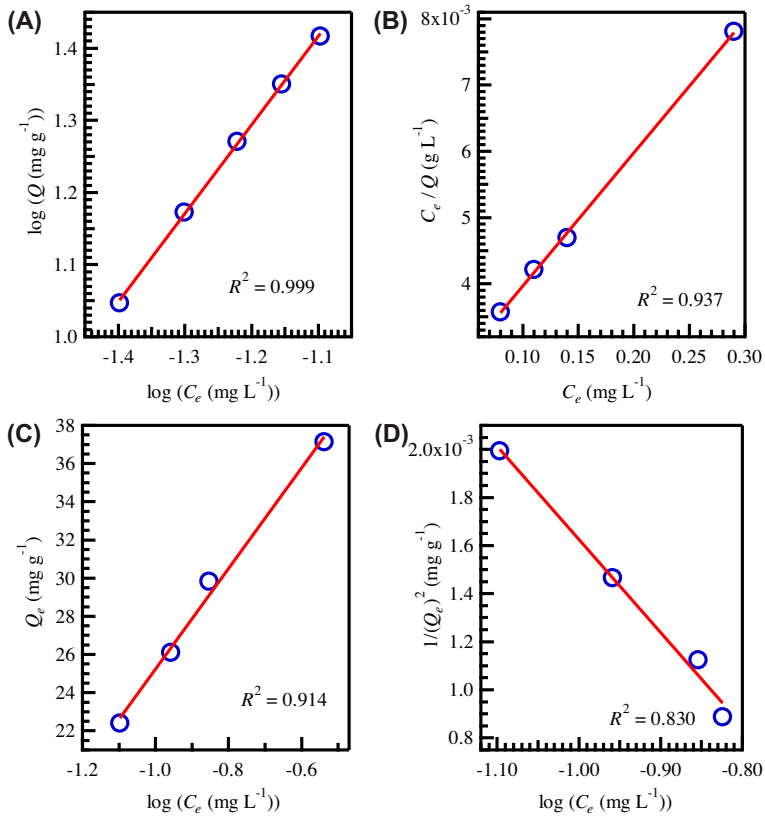

Fig. 6. Sorption isotherms for MB adsorption on Co_3O_4/SiO_2 nanocomposite, (A) Freundlich, (B) Langmuir, (C) Tempkin, and (D) Harkin–Jura. The solid lines are the linear fits.

Table 1
Fitting parameters for isotherm and kinetic models data

Model	Parameters	R^2
Freundlich	$K_F = 587.89\ mg\ g^{-1}$ $(L\ mg^{-1})^{1/n}$ $n = 0.813$	0.999
Langmuir	$K_L = 8.39\ L\ mg^{-1}$ $Q_{max} = 53.87\ mg\ g^{-1}$ $R_L = 3.97 \times 10^{-3}$	0.951
Tempkin	$K_T = 51.58\ L\ g^{-1}$ $B_T = 26.36\ J\ mol^{-1}$	0.914
Harkin–Jura	$A_{HJ} = 258.61\ mg^3\ g^{-2}\ L^{-1}$ $B_{HJ} = -0.58\ mg\ L^{-1}$	0.830
Pseudo-first-order	$K_1 = 0.03\ min^{-1}$ $Q_e = 6.23\ mg\ g^{-1}$	0.907
Pseudo-second-order	$K_2 = 0.01\ g\ mg^{-1}\ min^{-1}$ $Q_e = 25.42\ mg\ g^{-1}$	0.997
Intraparticle diffusion	$K_D = 0.63\ mg\ g^{-1}\ min^{1/2}$ $D = 19.01\ mg\ g^{-1}$	0.879
Simple Elovich	$K_E = 16.32\ mg\ g^{-1}\ min^{-1}$ $\beta = 9.70\ g\ mg^{-1}$	0.823

mordenite zeolite ($25.59\ mg\ g^{-1}$ or $8.0 \times 10^{-5}\ mol\ g^{-1}$) [26], carbon nanotubes ($35.0\ mg\ g^{-1}$) [27], mordenite nanocrystals ($38.38\ mg\ g^{-1}$ or $1.2 \times 10^{-4}\ mol\ g^{-1}$) [26], and Fe_3O_4/graphene nanocomposite ($45.27\ mg\ g^{-1}$) [28] at 298 K. The results indicate that Co_3O_4/SiO_2 nanocomposite is an excellent adsorbent and can be used to remove dyes from aqueous solutions. The coefficients of determination R^2 (0.937) of the Langmuir equation demonstrate that the adsorption of MB onto Co_3O_4/SiO_2 follows the Langmuir's model. The dimensionless equilibrium parameter (R_L), is calculated using Eq. (13) as [29]:

$$R_L = \frac{1}{1 + C_{max} K_L} \tag{13}$$

where C_{max} is the maximum initial concentration of MB ($mg\ L^{-1}$). R_L values between 0 and 1 indicate favorable adsorption. The R_L value here was found to be 3.97×10^{-3}.

Alternative sorption isotherm models, such as Tempkin and Harkin–Jura models, have been checked for the sake of comparison. The Tempkin model is expressed by Eq. (14) as [30]:

$$Q_e = \frac{R\,T}{2.303\,B_T} \log K_T + \frac{R\,T}{2.303\,B_T} \log C_e \tag{14}$$

where R is the universal gas constant ($8.314\ J\ mol^{-1}\ K^{-1}$), T is the absolute solution temperature (K), B_T is the Tempkin constant related to heat of sorption ($J\ mol^{-1}$), and K_T is the Tempkin isotherm constant ($L\ g^{-1}$). The linear relation obtained by plotting Q_e vs. $\log C_e$ is shown in Fig. 6(C). B_T and K_T are obtained to be $26.36\ J\ mol^{-1}$ and $51.58\ L\ g^{-1}$, respectively.

The Harkin–Jura model represented by Eq. (15) [30] has also been applied for these data

$$\frac{1}{Q_e^2} = \frac{B_{HJ}}{A_{HJ}} - \frac{1}{A_{HJ}} \log C_e \tag{15}$$

where A_{HJ} and B_{HJ} are Harkins–Jura constants. The results are shown in Fig. 6(D). The correlation coefficient for Freundlich isotherm ($R^2 = 0.999$) was the highest in comparison to the Langmuir, Temkin, and Harkins–Jura isotherms, which indicate that the Freundlich isotherm best represents the equilibrium adsorption of MB on Co_3O_4/SiO_2 nanocomposite.

3.4.5. Kinetic studies

The adsorption kinetics describes the rate of MB uptake on the nanocomposites, and this rate consequently controls the equilibrium time. The pseudo-first-order kinetic model of Lagergren may be represented by Eq. (16) as [24,27,28,31]:

$$\log (Q_e - Q_t) = \log Q_e - \frac{K_1}{2.303} t \tag{16}$$

where Q_e and Q_t are the amounts of MB in the solution ($mg\ g^{-1}$) at equilibrium and a time t, respectively. K_1 is the rate constant of pseudo-first-order adsorption (min^{-1}) and t is the time of adsorption (min). Fig. 7(A) shows a plot of $\log (Q_e - Q_t)$ vs. t. Linear fitting of the experimental data gave $K_1 = 0.03035\ min^{-1}$ and $Q_e = 6.23\ mg\ g^{-1}$.

The pseudo-second-order equation based on adsorption equilibrium capacity can be expressed by Eq. (17) as [24,27,31]:

$$\frac{t}{Q_t} = \frac{1}{K_2\,Q_e^2} + \frac{1}{Q_e} t \tag{17}$$

where K_2 is the rate constant of pseudo-second-order adsorption ($g\ mg^{-1}\ min^{-1}$). A linear relation was obtained when t/Q_t is plotted against t, as shown in Fig. 7(B). The K_2 was calculated as $0.01034\ g\ mg^{-1}\ min^{-1}$, and the Q_e value was $25.42\ mg\ g^{-1}$, which is very close to the experimental value of $25\ mg\ g^{-1}$. The pseudo-second-order kinetic equation best describes the sorption kinetics. These results support the chemisorptions of MB on Co_3O_4/SiO_2 nanocomposite [17].

Other kinetic models, such as intraparticle diffusion and Elovich models have been further

checked. The intraparticle diffusion model which elucidates the diffusion mechanism is expressed by Eq. (18) as [24,27]:

$$Q_t = K_D\, t^{1/2} + D \tag{18}$$

where K_D is the intraparticle diffusion rate constant (mg g^{-1} min$^{1/2}$) and the intercept D gives an idea about the thickness of the boundary layer. Plotting of Q_t vs. $t^{1/2}$ gives straight line as shown in Fig. 7(C). Linear fitting of the present data gives $K_D = 0.63248$ mg g^{-1} and $D = 19.008$, respectively.

The simple Elovich model is expressed by Eq. (19) in the form [24]:

$$Q_t = K_E + \frac{\beta}{2.303}\log t \tag{19}$$

where K_E represents the rate of chemisorption at zero coverage (mg g^{-1} min^{-1}) and β is related to the extent of surface coverage and activation energy for chemisorption (g mg^{-1}). When Q_t is plotted against log t, a linear relation is obtained as shown in Fig. 7(D). $K_E = 16.321$ mg g^{-1} min^{-1} and $\beta = 9.701$ g mg^{-1} were obtained from the intercept and slope of the line. All of the former parameters are re-summarized in Table 1. Among of all above models, the pseudo-second-order model is found to be the most appropriate model that can represent the experimental data.

3.4.6. Pore diffusion coefficient

The pore diffusion coefficient (D_p) can be calculated using Eq. (20) [26] assuming spherical geometry for the adsorbent as:

$$D_p = \frac{0.03\, r^2}{t_{1/2}} \tag{20}$$

where r is the adsorbent particle diameter (cm) and $t_{1/2}$ is the time for half adsorption (s). The r value is calculated from PS_{XRD} assuming spherical particle

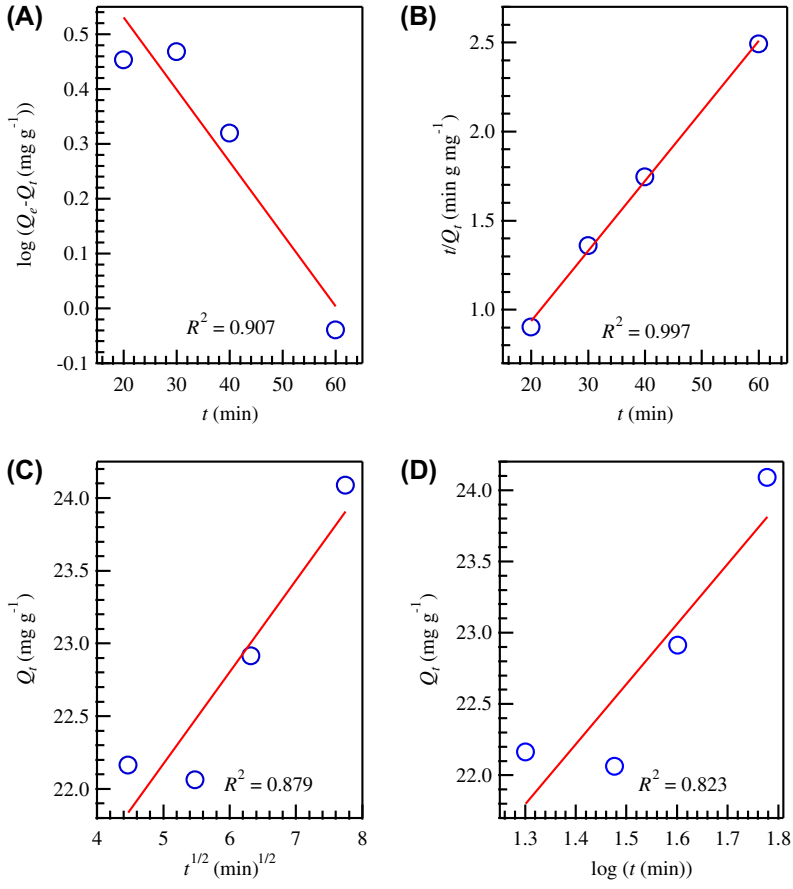

Fig. 7. Kinetic plots: (A) pseudo-first-order, (B) pseudo-second-order, (C) intraparticle diffusion, and (D) simple Elovich models for MB adsorption on Co_3O_4/SiO_2 nanocomposite. The solid lines are the linear fits.

shape ($r = 6.75 \times 10^{-7}$ cm). The $t_{1/2}$ is calculated from the rate constant of the second-order model (K_2) and the initial concentration (C_i) of MB (25 mg g^{-1}) as $t_{1/2} = 1/K_2 C_i$. For MB, a D_p value of 0.569×10^{-16} $cm^2 s^{-1}$ was obtained. The removal of MB by Co_3O_4/SiO_2 nanocomposite is little affected by pore diffusion process because of the D_p value is very small than the range of $10^{-11} - 10^{-13}$ $cm^2 s^{-1}$ [17,32,33].

4. Conclusion

Co_3O_4/SiO_2 nanocomposite has been prepared by novel aqueous solution method. XRD and FTIR data indicate the formation of pure nanocrystalline Co_3O_4 phase imbedded in an amorphous SiO_2 matrix. The removal of MB from aqueous solution by Co_3O_4/SiO_2 nanocomposite has been investigated under different experimental conditions in batch model. The obtained nanocomposite shows a good efficiency and high adsorption capacity for removal of MB from aqueous solutions. The removal percent of MB by Co_3O_4/SiO_2 has reached 95.7% and the adsorption capacity was 53.87 mg g^{-1}, which is larger than the adsorption capacity of MB on other materials. The kinetic of the adsorption process was best described by a pseudo-second-order rate equation. The calculated Q_e value based on the second-order model is in good agreement with the experimental one, supporting the chemisorption process.

Acknowledgment

The authors wish to express their thanks to Mr Emad Kamal for his technical support and discussion.

References

[1] L.S. Sales, P.A. Robles-Dutenhefner, D.L. Nunes, N.D.S. Mohallem, E.V. Gusevskaya, E.M.B. Sousa, Characterization and catalytic activity studies of sol–gel Co–SiO_2 nanocomposites, Mater. Charact. 50 (2003) 95–99.
[2] R. Xie, D. Li, B. Hou, J. Wang, L. Jia, Y. Sun, Silylated Co_3O_4–m–SiO_2 catalysts for Fischer–Tropsch synthesis, Catal. Commun. 12 (2011) 589–592.
[3] P. Shukla, H. Sun, S. Wang, H.M. Ang, M.O. Tadé, Nanosized Co_3O_4/SiO_2 for heterogeneous oxidation of phenolic contaminants in waste water, Sep. Purif. Technol. 77 (2011) 230–236.
[4] O.A. Fouad, G.A.M. Ali, M.A.I. El-Erian, S.A. Makhlouf, Humidity sensing properties of cobalt oxide/silica nanocomposites prepared via sol–gel and related routes, Nano 7(5) (2012) 1250038.
[5] X. Lu, G. Liang, Z. Sun, W. Zhang, Ferromagnetic Co/SiO_2 core/shell structured nanoparticles prepared by a novel aqueous solution method, Mater. Sci. Eng. B 117 (2005) 147–152.
[6] X. Lu, G. Liang, Q. Sun, C. Yang, The influence of silica matrix on the crystal structure and high frequency performance of cobalt nanoparticles, J. Solid State Chem. 183 (2010) 1555–1560.
[7] X.J. Yin, K. Peng, A.P. Hu, L.P. Zhou, J.H. Chen, Y.W. Du, Preparation and characterization of core–shell structured Co/SiO_2 nanosphere, J. Alloys and Compd. 479 (2009) 372–375.
[8] O.A. Fouad, S.A. Makhlouf, G.A.M. Ali, A.Y. El-Sayed, Cobalt/silica nanocomposite via thermal calcination-reduction of gel precursors, Mater. Chem. Phys. 128 (2011) 70–76.
[9] S. Lambert, K.Y. Tran, G. Arrachart, F. Noville, C. Henrist, C. Bied, J.J.E. Moreau, M.W.C. Man, B. Heinrichs, Tailor-made morphologies for Pd/SiO_2 catalysts through sol–gel process with various silylated ligands, Microporous Mesoporous Mater. 115 (2008) 609–617.
[10] M. Domínguez, E. Taboada, E. Molins, J. Llorca, Co–SiO_2 aerogel-coated catalytic walls for the generation of hydrogen, Catal. Today 138 (2008) 193–197.
[11] C. Sellmer, S. Decker, N. Kruse, CO hydrogenation over Co/SiO_2: Catalytic tests and surface analysis of adsorbed hydrocarbons, Catal. Lett. 52 (1998) 131–137.
[12] M.L. Kantam, B.P.C. Rao, R.S. Reddy, N.S. Sekhar, B. Sreedhar, B.M. Choudary, Aerobic epoxidation of olefins catalyzed by Co–SiO_2 nanocomposites, J. Mol. Catal. A: Chem. 272 (2007) 1–5.
[13] M.M. El-Sheekh, M.M. Gharieb, G.W. Abou-El-Souod, Biodegradation of dyes by some green algae and cyanobacteria, Int. Biodeterior. Biodegrad. 63 (2009) 699–704.
[14] P. Cañizares, F. Martínez, C. Jiménez, J. Lobato, M.A. Rodrigo, Coagulation and electrocoagulation of wastes polluted with dyes, Environ. Sci. Technol. 40 (2006) 6418–6424.
[15] I.A. Salem, M. El-Maazawi, Kinetics and mechanism of color removal of methylene blue with hydrogen peroxide catalyzed by some supported alumina surfaces, Chemosphere 41 (2000) 1173–1180.
[16] C.-H. Weng, Y.-F. Pan, Adsorption of a cationic dye (methylene blue) onto spent activated clay, J. Hazard. Mater. 144 (2007) 355–362.
[17] D. Kavitha, C. Namasivayam, Experimental and kinetic studies on methylene blue adsorption by coir pith carbon, Bioresour. Technol. 98 (2007) 14–21.
[18] R. Han, Y. Wang, W. Zou, Comparison of linear and nonlinear analysis in estimating the Thomas model parameters for methylene blue adsorption onto natural zeolite in fixed-bed column, J. Hazard. Mater. 145 (2007) 331–335.
[19] J.L. Gurav, A.V. Rao, A.P. Rao, D.Y. Nadargi, S.D. Bhagat, Physical properties of sodium silicate based silica aerogels prepared by single step sol–gel process dried at ambient pressure, J. Alloys Compd. 476 (2009) 397–402.
[20] T.J.B. Holland, S.A.T. Redfern, Unit cell refinement from powder diffraction data: The use of regression diagnostics, Mineral. Mag. 61 (1997) 65–77.
[21] P. Muralidharan, M. Venkateswarlu, N. Satyanarayana, Sol–gel synthesis, characterization and impedance studies of lithium borosilicate glass, Mater. Res. Bull. 39 (2004) 1753–1762.

[22] G. Ortega-Zarzosa, C. Araujo-Andrade, M.E. Compeán-Jasso, J.R. Martínez, Cobalt oxide/silica xerogels powders: X-ray diffraction, infrared and visible absorption studies, J. Sol–Gel Sci. Technol. 24 (2002) 23–29.
[23] K.S.W. Sing, D.H. Everett, R.A.W. Haul, L. Moscou, R.A. Pierotti, J. Rouquerol, T. Siemieniewska, Reporting physisorption data for gas/solid systems with special reference to the determination of surface area and porosity (Recommendations 1984), Pure Appl. Chem. 57 (1985) 603–619.
[24] M.F. Elkady, M.M. Mahmoud, H.M. Abd-El-Rahman, Kinetic approach for cadmium sorption using microwave synthesized nano-hydroxyapatite, J. Non-Cryst. Solids 357 (2011) 1118–1129.
[25] A. Mittal, V.K. Gupta, A. Malviya, J. Mittal, Process development for the batch and bulk removal and recovery of a hazardous, water-soluble azo dye (metanil yellow) by adsorption over waste materials (bottom ash and de-oiled soya), J. Hazard. Mater. 151 (2008) 821–832.
[26] S. Sohrabnezhad, A. Pourahmad, Comparison absorption of new methylene blue dye in zeolite and nanocrystal zeolite, Desalination 256 (2010) 84–89.
[27] Y. Yao, F. Xu, M. Chen, Z. Xu, Z. Zhu, Adsorption behavior of methylene blue on carbon nanotubes, Bioresour. Technol. 101 (2010) 3040–3046.
[28] Y. Yao, S. Miao, S. Liu, L.P. Ma, H. Sun, S. Wang, Synthesis, characterization, and adsorption properties of magnetic Fe_3O_4@graphene nanocomposite, Chem. Eng. J. 184 (2012) 326–332.
[29] W. Li, L. Zhang, J. Peng, N. Li, S. Zhang, S. Guo, Tobacco stems as a low cost adsorbent for the removal of Pb(II) from wastewater: Equilibrium and kinetic studies, Ind. Crops Prod. 28 (2008) 294–302.
[30] A.M.M. Vargas, A.L. Cazetta, M.H. Kunita, T.L. Silva, V.C. Almeida, Adsorption of methylene blue on activated carbon produced from flamboyant pods (Delonix regia): Study of adsorption isotherms and kinetic models, Chem. Eng. J. 168 (2011) 722–730.
[31] A. Mittal, J. Mittal, A. Malviya, V.K. Gupta, Adsorptive removal of hazardous anionic dye "congo red" from wastewater using waste materials and recovery by desorption, J. Colloid Interface Sci. 340 (2009) 16–26.
[32] M.A. Al-Ghouti, M.A.M. Khraisheh, M.N.M. Ahmad, S. Allen, Adsorption behaviour of methylene blue onto Jordanian diatomite: A kinetic study, J. Hazard. Mater. 165 (2009) 589–598.
[33] V.K. Gupta, B. Gupta, A. Rastogi, S. Agarwal, A. Nayak, A comparative investigation on adsorption performances of mesoporous activated carbon prepared from waste rubber tire and activated carbon for a hazardous azo dye-acid blue 113, J. Hazard. Mater. 186 (2011) 891–901.